

Radiated Emissions of an Electric Drive System Estimated on a Bench Using Disturbance Currents and Transfer Functions

Daniel Schneider, Michael Beltle, Martin Siegel, Stefan Tenbohlen, *Member, IEEE*, and Wolfgang Köhler

Abstract—Electric drive systems are going to be the future of the automotive industry. Electromagnetic compatibility (EMC) issues and challenges arise with its growing entry into modern cars. This contribution provides an overview of the field dominating disturbance currents of an automotive high-voltage (HV) power inverter within an electric drive system. In order to minimize the cost and time needed for EMC measurements and engineering, a precompliance measurement method is introduced and applied to the inverter's setup. The method presented allows the calculation of radiated emissions, according to CISPR 25, needed during the development process without the need for an expensive anechoic chamber. Transfer functions in combination with measured disturbance currents on the attached HV harnesses are used to obtain a cost-efficient estimation of the radiated emissions occurring during a component test. Its theory is discussed and demonstrated using a derived model. The method is verified using a rudimentary test setup, which represents a distributed system, and is later validated by the active electric drive system test setup introduced. Examinations of repeatability and reproducibility of disturbance current measurements as well as applied EMC counter measures complete the contribution.

Index Terms—Automotive high-voltage (HV) power inverter, CISPR 25, distributed system, electric drive system, estimation, precompliance, radiated emission, transfer function.

I. INTRODUCTION

THE increasing electrification in the automotive industry accompanied by high complexity leads to a growing demand for electromagnetic compatibility (EMC) engineering and EMC measurements. First, each electric component has to be tested according to standards, such as CISPR 25 [1], in a component test, and second, assembled in a car, for a vehicle test. These tests are the generally accepted main tool for investigating EMC performance. Each test has to be organized, a test facility has to be booked, and the component and its peripheral equipment have to be ready in time. This procedure occurs multiple times, depending on changes of the component during the development process and its different prototype stages, which is costly and time consuming. Hence, alternatives, commonly

called precompliance methods, with the objective of giving an estimation of the result expected during standard measurements are desired [2]. Such EMC precompliance methods have to be practical and easy to apply during the development process giving a reliable estimation with an accuracy of 10 dB or better. They should not be regarded as a full replacement of the traditional measurements, but they have to be considered as an additional tool between the design process and the series production to ensure the EMC of a component. The advantages of such tools are fast and early measurement results and a minimization of the expense on measurement time for iterative tests in certified test sites. This applies especially for the high-priced radiated emission measurements on which this paper focuses.

Standard radiated emission tests for automotive components are defined in [1]. Those measurements take place in absorber-lined shielded enclosures (ALSE). The test setup is placed on a metallic table bonded to the enclosure acting as a ground reference. It consists of the device under test (DUT), its cable harness, a load, optional line impedance stabilization networks (LISNs), control units, and power supplies. The measurement antenna is positioned one meter in front of the test setup. Monopole, biconical, or log-periodic antennas are used as measurement systems depending on the frequency range of interest. EMI test receivers are used for recording the antenna voltage, which is proportional to the electric field strength. In summary, the test infrastructure necessary is complex and expensive, and thus, the access to such measurement facilities is limited.

One type of precompliance tool for predicting radiated emissions is a full-field simulator using, for example, the method of moments. Simulations need a model of the component to be examined and its setup environment, including the measurement equipment, for increased accuracy. All those aspects require a high modeling effort and a lot of knowhow. The main advantage of simulations is the decoupling from real hardware. Simulations can be initiated long before the first real hardware exists. Another possibility of estimating radiated emissions is a hybrid approach. This uses a calculation model in combination with measurements on a bench, which are easy to perform. These approaches mainly use analytic models relying on Hertzian dipole arrays, which represent the cable harness as a sole radiator carrying common-mode currents and include parts of the test setup's geometry. They have often been investigated, e.g., in [3]–[8]. The disadvantages of such approaches are the lack of the near field coupling of the setup with the spatially distributed antenna structure and the ALSE characteristic. The field is calculated at

Manuscript received April 14, 2014; revised June 25, 2014 and September 2, 2014; accepted February 5, 2015. Date of publication March 18, 2015; date of current version June 11, 2015. This work was supported by Robert Bosch GmbH.

The authors are with the Department IEH, University of Stuttgart, Stuttgart 70569, Germany (e-mail: daniel.schneider@ieh.uni-stuttgart.de; michael.beltle@ieh.uni-stuttgart.de; martin.siegel@ieh.uni-stuttgart.de; stefan.tenbohlen@ieh.uni-stuttgart.de; wolfgang.koehler@ieh.uni-stuttgart.de).

Color versions of one or more of the figures in this paper are available online at <http://ieeexplore.ieee.org>.

Digital Object Identifier 10.1109/TEMC.2015.2401735

the position of the antenna feeding point. The influence of the measurement table is implemented by the image theory, which is only correct for infinite ground planes [9]. Moreover, reflection from the grounded floor is omitted completely. Housings of the DUTs and of accessorial equipment are not taken into account, neither are diffraction and scattering effects. Therefore, they are limited to simple setups. A numerical method applying Huygens' principle, which can comprise the whole setup except for the ALSE, is presented in [10].

The drawback of missing aspects can be eliminated by the use of measurable transfer functions (TFs), including the entire system in combination with disturbance current measurements on the harnesses attached to the component tested [11]. TFs represent the correlation between disturbance currents in an ALSE setup and the related measurable electric field strength. Current measurements for the field estimation can be conducted in simple laboratory setups. Necessary TFs are available from previous similar projects or have to be generated during the first measurements of a component in an ALSE. The main advantage of the TF method is that there is no need for excessive modeling. All the information of the test setup with the ALSE and measurement equipment is captured in the TFs. Furthermore, engineers are usually accustomed to measurement-based approaches. Investigations of the method in the automotive area show its applicability [12], [13] for nondistributed systems with single and multiple segment TFs. It is shown that for frequencies below 30 MHz good results can be achieved.

This contribution adapts and applies the TF method as a precompliance tool to one of the most challenging automotive EMC areas nowadays: the electrification of the drive system. Here, as well as in any other EMC areas, fast and cost-efficient EMC engineering is desired. The main parts of drive systems are: a high-voltage (HV) battery, an HV power inverter, and an electric drive machine. The interconnection is mainly realized by shielded coaxial HV cables. The inverters applied convert the HVDC of the traction network (TN) from the HV battery into a three-phase ac on the phase network (PN) for the drive machine. Those inverters represent the most critical disturbance source [14] due to fast slew rates of the insulated gate bipolar transistors (IGBTs) applied within the electric drive system. Fast slew rates are mandatory to reduce power dissipation.

A test setup for an electric drive system is introduced in Section II, which allows the characterization of only the EMC performance of the HV inverter. The system regarded consists of a preseries sample of an HV inverter, an HV source, an HV LISN, a 12 V source, and LISNs for the low-voltage (LV) supply of the inverter's electronics, and an electric machine emulation (EME) (see Fig. 1). Its disturbance currents and current paths are examined in Section III. The principle of the TF method for distributed systems is explained. Its theory is discussed and verified by a SPICE simulation in Section IV. The frequency range considered is between 0.15 and 30 MHz, which is the range of the main emissions of this inverter. The application of the method will be verified by a rudimentary nonshielded setup in Section V, followed by a validation using an active inverter setup in Section VI. Repeatability and reproducibility analysis concerning the current probe measurements, this method is based

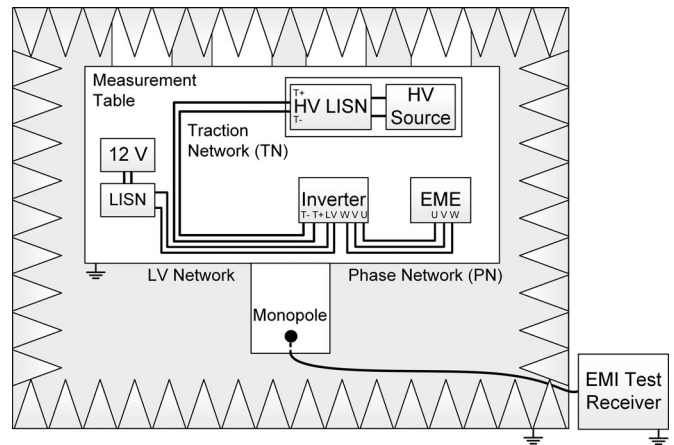


Fig. 1. Block diagram of the drive system setup investigated.

on, are presented in Section VII and an example concerning applied EMC counter measures are presented in Section VIII.

II. DRIVE SYSTEM SETUP

The setup investigated is an extension of the setup used in [15]. The central element is a modified preproduction sample of an HV inverter. This inverter has a voltage range of 150–430 V dc from the HV battery or HV LISN over the TN. It is software adjusted, so it can be operated in a measurement facility, which is not equipped with an HV source. A minimum of 20 V dc for the inverter's intermediate circuit voltage is needed, which has to be applied at the terminals T+ and T- of the TN. Furthermore, no active cooling of the inverter is required. This setting allows an active operational state of the inverter without any additional communication, such as CAN bus or sensors. This assigns the inverter and its switching IGBTs as the main noise source. The operation mode of the inverter is set to a zero-ampere mode, which is the worst case concerning common mode as the IGBTs are switching simultaneously. A 12 V car battery in combination with LV LISNs is used as the power supply for the internal control unit. Therefore, the terminals 15 (ignition, switched on plus), 30 (battery plus), and 31 (battery minus) of the inverter are connected to the two LV LISNs for plus and minus power supply. This LV harness has a length of 1.5 m. It is placed, according to [1], 5 cm above the metallic measurement table and 10 cm away from the table's edge. The inverter's terminals T+ and T- are supplied over an HV LISN connected to a 24 V battery. The HV LISN consists of a shielding box containing two LISNs. Due to the influence observed of the connection cables between HV LISN and the 24 V battery on the TF generation, the battery is also placed into the shielding box of the HV LISN. The inverter is equipped with N-type adaptors at its terminals T+, T-, U, V, and W. This allows measurements, which lead to a passive high-frequency emulation of the inverter [16].

A further N-type connector is mounted to the inverter's housing, which acts as a feeding connector for an external signal source. This feeding connector is later used for TF generation and verification purposes. An EME is used as load for the inverter, representing the simplified high-frequency properties of

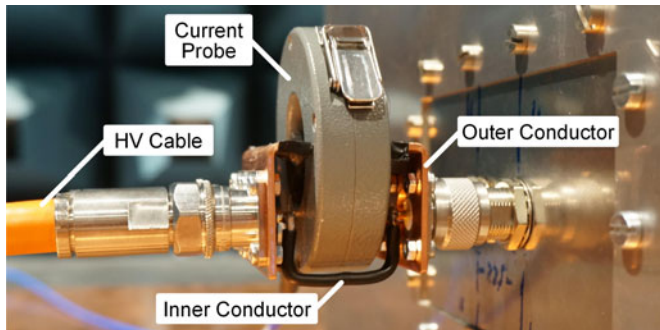


Fig. 2. Adaptor for shield current measurements on the traction network with current probe applied.

an electric drive machine. The EME is set up in a shielded housing. A standard equivalent circuit with three star-connected randomly chosen inductors ($L = 5 \mu\text{H}$) is set up on a printed-circuit board (PCB). In order to emulate the dominating parasitic capacitances between the terminals U, V, W, and the ground, capacitors ($C = 10 \text{ nF}$) are placed at the three inputs of the emulation to the ground. The applied HV cables and the terminals of the HV LISN and the EME are equipped with N-type connectors instead of the automotive HV connectors for easy laboratory use. The shielded coaxial HV cables, with a wire cross section of 25 mm^2 , have a length of 3.3 m for the TN and 0.5 m for the PN. They are positioned 5 cm above the table and 10 cm away from the table's edge. Due to the shielded networks and the close cable running of the networks, the common-mode currents are expected to dominate the electric field strength. Hence, differential-mode currents are neglected in the following analysis. The position of the HV LISN is not compliant with the standard due to the length of the TN and the limited size of the measurement table. In order to measure the currents from the HV LISN and the EME to the ground, each is set up on one single metallic bolt connected to the ground. Additional adaptors between the HV LISN and the TN's HV cables and between the EME and the PN's HV cables allow measurements of currents on the shielding. As an example, Fig. 2 shows the adaptor used at the TN side with a mounted current probe. The adaptors can be shielded entirely with U-shaped copper brackets. The measurement table is laminary bonded to the shielded enclosure with four copper sheets, each 40 cm wide, at the rear side of the table. This assures small contact impedance and a good ground concept, which is important for a successful pre-compliance result compared to real measurements. The setup introduced is situated in an ALSE (see Fig. 3).

III. DISTURBANCE CURRENTS ON THE NETWORKS

The field-generating disturbance currents have to be examined in order to understand the radiated emissions of the setup. Fig. 4 shows the disturbance currents of the active inverter measured with a current probe positioned at different points in the setup. The six positions can be seen in a reduced block diagram in Fig. 5. The currents $I_{\text{HV LISN}}(f)$ and $I_{\text{TN GND}}(f)$ are equal and represent a part of the disturbance current generated by the switching IGBTs. They flow through the TN and back to the

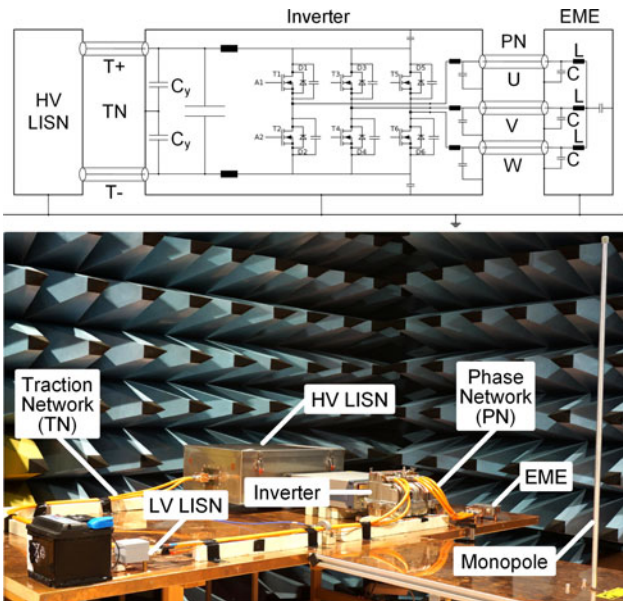


Fig. 3. Equivalent circuit (top) and photograph (bottom) of the measurement setup of the investigated electric drive system in an ALSE.

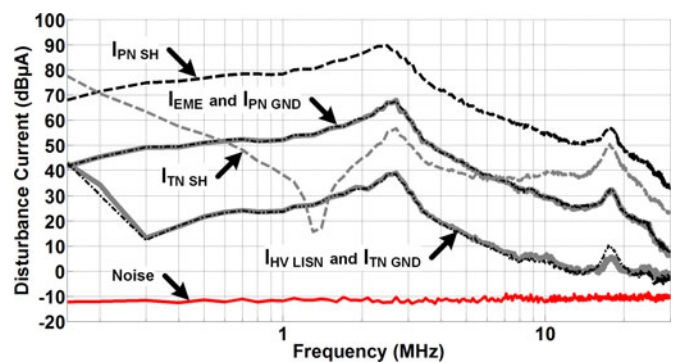


Fig. 4. Disturbance currents measured at specific points in the setup.

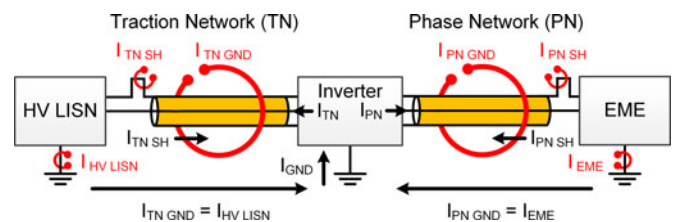


Fig. 5. Current probe measurement points in a reduced block diagram.

source over the ground plane measurement table. These currents are called ground currents. $I_{\text{TN SH}}(f)$ is the other part of the disturbance current in the TN, which has its return path over the shield of the coaxial cables. This current is more than 10 dB higher in amplitude than the ground current for most frequencies, except in between 0.6 and 6 MHz. The currents $I_{\text{EME}}(f)$ and $I_{\text{PN GND}}(f)$ represent the part of the disturbance current of the PN flowing back to the source over the ground plane. The part flowing through the shielding of the PN $I_{\text{PN SH}}(f)$ is up to 30 dB higher in amplitude. Fig. 4 provides two main observations: The disturbance currents on the inner conductors split

into two parts, as in (1) and (2). The main part of the disturbance currents $I_{TN}(f)$ and $I_{PN}(f)$ of each network flows back over the HV cable's shielding, which is generally dependent on frequency, length of the harness, and distance of the harness to the ground [17], [18]. The second part, flowing back over the ground $I_{GND}(f)$, can be measured with a current probe around the entire TN and around the entire PN, respectively [see (3)].

$$I_{TN}(f) = I_{TN\ SH}(f) + I_{TN\ GND}(f) \quad (1)$$

$$I_{PN}(f) = I_{PN\ SH}(f) + I_{PN\ GND}(f) \quad (2)$$

$$I_{GND}(f) = I_{TN\ GND}(f) + I_{PN\ GND}(f) \quad (3)$$

IV. METHOD OF TRANSFER FUNCTIONS

A. Principle of Transfer Functions

The radiated electric field strength of a component in a component test can be calculated on the basis of field-dominating common-mode currents [19] using an analytic model or TFs of the setup. The analytic approach is practical for simple setups. Modeling of complex setups with ALSE and antenna characteristics, spatial current distributions along the entire measurement setup, as well as diffraction and scattering is beyond practicability if performed analytically. This disadvantage can be eliminated by numerical solutions or TFs. A TF represent the correlation between the electric field strength $E(f)$ and its appending disturbance current $I(f)$. They can be obtained by a measurement procedure including current probe measurements on a component's cable harness and an electric field strength measurement with an antenna. These measurements can be performed by an EMI test receiver. For this purpose, the setup of a component inside an ALSE is excited by a tracking generator (TG) instead of the DUT feeding the harness with a common-mode current. With the measured peak values of the electric field strength $E(f)$ and the disturbance current $I(f)$, TFs can be calculated as

$$TF(f) = \frac{E(f)}{I(f)} = \frac{U_{Ant}(f)}{U_{CP}(f)} \cdot AF(f) \cdot Z_T(f) \quad (4)$$

with the antenna peak voltage $U_{Ant}(f)$, the current probe peak voltage $U_{CP}(f)$, the antenna factor $AF(f)$, and the transimpedance $Z_T(f)$ of the current probe.

An estimation of a component's radiated emission is now possible without an ALSE. For this purpose, the DUT is arranged on a metal-plated bench in a simple laboratory attached to the according setup, as used for the TF generation, replacing the signal generator. The disturbance current $I_{DUT}(f)$ has to be measured by an EMI test receiver with peak detector at the same position as during the TF generation. With the TF obtained, the peak value of the electric field strength $E_{calc\ DUT}(f)$ can then be estimated by (5). This is a valid procedure as long as the current distribution of the DUT is comparable to the one implemented in the TF [13].

$$E_{calc\ DUT}(f) = TF(f) \cdot I_{DUT}(f) \quad (5)$$

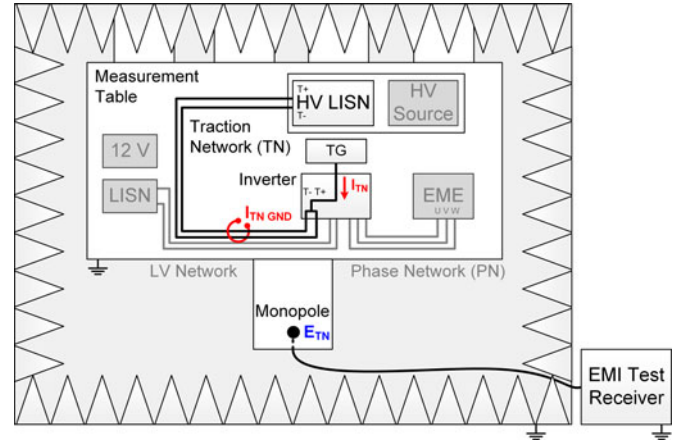


Fig. 6. Setup for the TF generation of the traction network (TN) with a tracking generator (TG).

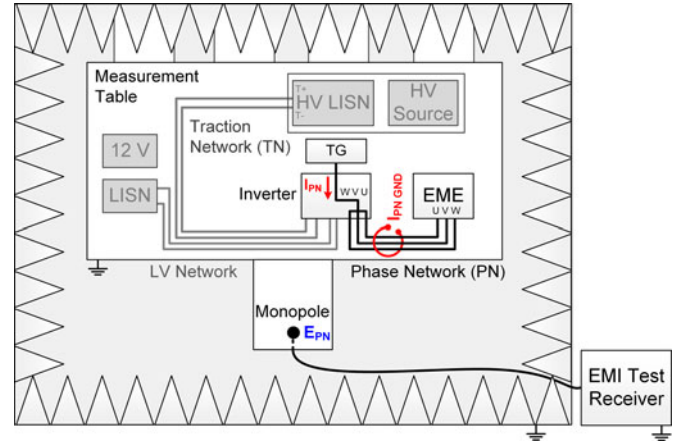


Fig. 7. Setup for the TF generation of the phase network (PN) with a tracking generator (TG).

B. Combined Transfer Functions

The drive system setup regarded consists of two main branches: the TN, connecting the inverter with the HV source, and the PN, connecting the inverter with the electric drive machine. Two independent TFs representing both subsystems have to be generated, one for each branch. The cable running of the networks is important for obtaining correct estimation results as the TF procedure bases on dominating common-mode currents. The single cables of each network have to be close to each other so the contribution of possible differential mode currents to the electric field is minimized. Because the housing of the inverter is quite big and defines the position of the HV cables, it has to be implemented into the TFs for accurate results. Therefore, an inverter is modified, making it possible to excite the TN of the setup in an ALSE over its terminals T+ and T- with the common-mode signal $I_{TN}(f)$ on the two inner conductors of the shielded HV cables. The same applies to the PN concerning its terminals U, V, and W with the common-mode signal $I_{PN}(f)$. A TG is used as a signal source. Fig. 6 and 7 show the block diagrams of both setups. The inner conductor of the coaxial feeding cable from the TG is connected via an N-type feeding

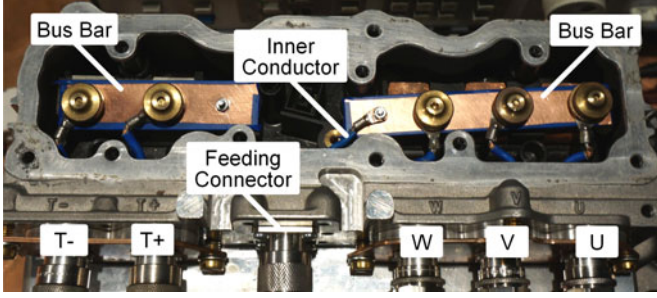


Fig. 8. Top view of the inverter: Example of the interconnection with bus bars for the phase network (PN) excitation over U, V, and W.

connector to bus bars for excitation. The feeding connector is assembled to the grounded housing of the inverter. This allows the connection of the TN, the PN or both simultaneously with the excitation signal and reference to the ground, compare Fig. 8. Internal inverter electronics are insulated and not connected to the bus bars or the terminals T+, T-, U, V, and W. There are no additional voltage sources connected to the inverter during the generation process. The TG is supplied by a separate insulating transformer and the connection cable between TG and feeding connector is equipped with ferrites suppressing unwanted radiation effects and current paths. Successive measurements of the resulting ground currents $I_{TN\ GND}(f)$ and $I_{PN\ GND}(f)$ plus the according field strengths $E_{TN}(f)$ and $E_{PN}(f)$ with an EMI test receiver with peak detector lead to the TFs

$$\begin{aligned} TF_{TN}(f) &= \frac{E_{TN}(f)}{I_{TN\ GND}(f)} \\ &= \frac{U_{Ant\ TN}(f)}{U_{CP\ TN\ GND}(f)} \cdot AF(f) \cdot Z_T(f) \quad (6) \end{aligned}$$

$$\begin{aligned} TF_{PN}(f) &= \frac{E_{PN}(f)}{I_{PN\ GND}(f)} \\ &= \frac{U_{Ant\ PN}(f)}{U_{CP\ PN\ GND}(f)} \cdot AF(f) \cdot Z_T(f). \quad (7) \end{aligned}$$

By using these TFs and two disturbance current measurements $I_{TN\ GND\ DUT}(f)$ on the TN and $I_{PN\ GND\ DUT}(f)$ on the PN, respectively, the radiated electric field strength of an active inverter being the DUT can be calculated. The application of the superposition principle in (8) on the two calculated electric field parts $E_{calc\ TN\ DUT}(f)$ and $E_{calc\ PN\ DUT}(f)$ leads to the calculated field strength

$$\begin{aligned} E_{calc\ DUT}(f) &= E_{calc\ TN\ DUT}(f) + E_{calc\ PN\ DUT}(f) \\ &= TF_{TN}(f) \cdot I_{TN\ GND\ DUT}(f) \\ &\quad + TF_{PN}(f) \cdot I_{PN\ GND\ DUT}(f). \quad (8) \end{aligned}$$

Due to the fact that the setup can be considered as electrically small [3] and only near-field coupling occurs in the frequency range up to 30 MHz, phase information will be neglected for the TFs. Further, the phase of the disturbance currents $I_{TN\ GND\ DUT}(f)$ and $I_{PN\ GND\ DUT}(f)$ is neglected as EMI test receiver measurements give only absolute values. This leads to a worst case approximation of the electric field strength. As the

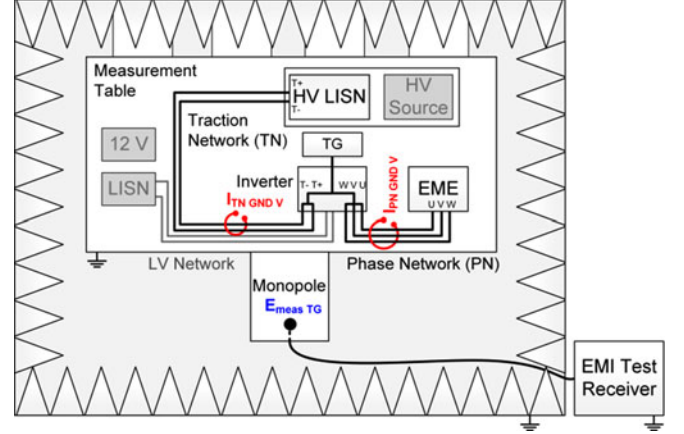


Fig. 9. Setup for the verification of a combined transfer function set using a tracking generator (TG) as DUT.

field is measured with a 1-m-long vertical monopole antenna, the dominating field coupling mechanism is capacitive. The LV cable harness is not considered by a separate TF because of its observed minimal influence on the field strength of the active inverter setup.

C. Verification Process of Combined Transfer Function Sets

The TN and the PN are excited simultaneously with a TG acting as DUT to verify a generated combined TF set (see Fig. 9). This is achieved by one bus bar connecting T+, T-, U, V, and W to the inner conductor of the feeding connector. Voltage sources are not connected to the setup, and internal inverter electronics are insulated from the terminals. This leads to the disturbance currents $I_{TN\ GND\ V}(f)$ and $I_{PN\ GND\ V}(f)$ shown in Fig. 9. These ground disturbance currents are measured sequentially with a current probe at the same positions as during the TF generation. A field strength measurement $E_{meas\ TG}(f)$ with a monopole serves as reference. The currents measured with the corresponding TFs inserted into (8) lead to the verification result $E_{calc\ TG}(f)$. This result compared to the reference measurement $E_{meas\ TG}(f)$ indicates the correctness of the TFs and the measurement procedure.

D. Modeling of the Setup–Antenna Coupling Mechanism

A model of the system has to be derived as an explanation for the application of the superposition principle in (8). The quantity regarded is the electric field strength, which is proportional to the antenna voltage measured by a monopole antenna representing an electric field probe. Both are linked through the antenna factor. The antenna factor $AF(f) = 1/m$ is chosen as a simplification. Thus, only the antenna voltages are considered in the following. The antenna input impedance $Z_{Ant}(f)$ of the monopole is modeled with a capacitor C_{Ant} in parallel to a high ohmic resistor R_{Ant} . The monopole is in the near-field area of the harnesses because of the geometrical size of the whole setup. Hence, the coupling mechanism between the setups and the antenna is capacitive. It can be represented by the coupling capacitors C_{TN} for the TN and C_{PN} for the PN. Fig. 10 shows

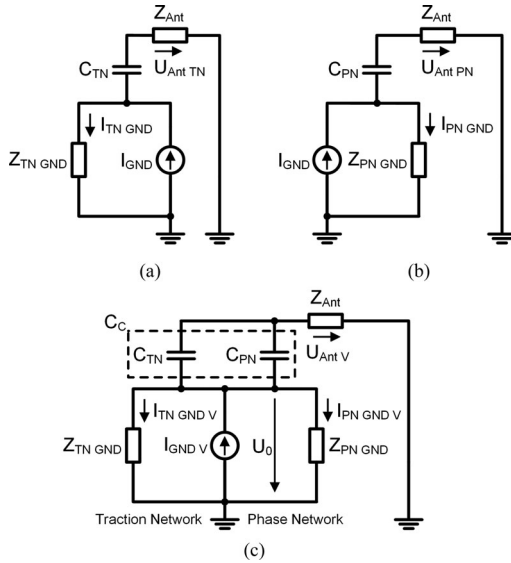


Fig. 10. Schematic of the electric models for the (a) traction network (TN) setup, (b) the phase network (PN) setup, and (c) the verification setup.

the schematics of the models for the two TF setups in (a) and (b) and the verification setup in (c). The impedance $Z_{TN\ GND}(f)$ comprises the HV LISNs and the ground impedance seen by the ground current of the TN. The impedance $Z_{PN\ GND}(f)$ comprises the EME and the ground impedance seen by the ground current of the PN. The radiation is caused by the potential difference of the harnesses to the monopole generated by the ground currents flowing through the networks. Shield currents of the coaxial HV cables compensate their electric field in relation to the monopole with its counterpart on the inner conductor. This is because of the small cable diameter compared to the distance between cable and monopole and its equal amplitude with opposite sign [20]. Hence, a model representing the coupling between setup and antenna only includes the ground current $I_{GND}(f)$ as source. The mathematical TFs according to the schematics shown in Fig. 10(a) and (b) are given by (9) and (10). Coupling effects between the two TF setups are neglected.

$$TF_{TN}(f) = \frac{U_{Ant\ TN}(f)}{I_{TN\ GND}(f)} = \frac{Z_{TN\ GND}(f) \cdot Z_{Ant}(f)}{Z_{C_{TN}}(f) + Z_{Ant}(f)} \quad (9)$$

$$TF_{PN}(f) = \frac{U_{Ant\ PN}(f)}{I_{PN\ GND}(f)} = \frac{Z_{PN\ GND}(f) \cdot Z_{Ant}(f)}{Z_{C_{PN}}(f) + Z_{Ant}(f)} \quad (10)$$

$Z_{C_{TN}}(f)$ and $Z_{C_{PN}}(f)$ are the impedances of the coupling capacitors C_{TN} and C_{PN} . The estimation of the antenna voltage $U_{Ant\ calc}(f)$ of the verification setup in Fig. 10(c) can be determined by (11) using the TFs and the verification currents $I_{TN\ GND\ V}(f)$ and $I_{PN\ GND\ V}(f)$ out of the schematic in Fig. 10(c) according to (8)

$$U_{Ant\ calc}(f) = \frac{Z_{TN\ GND}(f) \cdot Z_{Ant}(f)}{Z_{C_{TN}}(f) + Z_{Ant}(f)} \cdot I_{TN\ GND\ V}(f) + \frac{Z_{PN\ GND}(f) \cdot Z_{Ant}(f)}{Z_{C_{PN}}(f) + Z_{Ant}(f)} \cdot I_{PN\ GND\ V}(f). \quad (11)$$

The reference antenna voltage $U_{Ant\ V}(f)$ of the verification setup in Fig. 10(c) is derived depending on the currents $I_{TN\ GND\ V}(f)$ and $I_{PN\ GND\ V}(f)$ according to

$$U_{Ant\ V}(f) = \frac{Z_{Ant}(f)}{Z_C(f) + Z_{Ant}(f)} \cdot \frac{Z_{TN\ GND}(f) \cdot Z_{PN\ GND}(f)}{Z_{TN\ GND}(f) + Z_{PN\ GND}(f)} \cdot [I_{TN\ GND\ V}(f) + I_{PN\ GND\ V}(f)] \quad (12)$$

with $Z_C(f)$ as the parallel circuit of $Z_{C_{TN}}(f)$ and $Z_{C_{PN}}(f)$ comprising the overall coupling capacitance C_C between setup and monopole.

$U_{Ant\ calc}(f)$ and $U_{Ant\ V}(f)$ have to be equal to proof the application of the superposition principle. This can be shown under the following assumption:

$$Z_{C_{TN}}(f), Z_{C_{PN}}(f) > Z_C(f) > Z_{Ant}(f). \quad (13)$$

This assumption is adequate, because the coupling capacitances between the networks and the monopole are significantly smaller than the input capacitance of the monopole itself. The coupling capacitances C_{TN} and C_{PN} are in the range of several 100 fF. The input capacitance of a monopole antenna is comprised of the self-capacitance of the rod and the capacitance of the matching unit's high impedance input circuitry. Both together are at least 10 pF, representing the self-capacitance of a 1 m rod to the ground. This value is the worst case leading to the highest possible value for the antenna impedance. With (13), $Z_{Ant}(f)$ can be neglected in the denominators of (11). Additional substitution of $I_{TN\ GND\ V}(f)$ and $I_{PN\ GND\ V}(f)$ with $U_0(f)/Z_{TN\ GND}(f)$ and $U_0(f)/Z_{PN\ GND}(f)$, respectively, in (11), leads to

$$U_{Ant\ calc}(f) = Z_{Ant}(f) \cdot U_0(f) \cdot \left[\frac{1}{Z_{C_{TN}}(f)} + \frac{1}{Z_{C_{PN}}(f)} \right] = Z_{Ant}(f) \cdot U_0(f) \cdot \frac{1}{Z_C(f)}. \quad (14)$$

Extending (14) with $(Z_{TN\ GND}(f) + Z_{PN\ GND}(f))/(Z_{TN\ GND}(f) + Z_{PN\ GND}(f))$ results in

$$U_{Ant\ calc}(f) = \frac{Z_{Ant}(f)}{Z_C(f)} \cdot \frac{U_0(f) \cdot Z_{TN\ GND}(f)}{Z_{TN\ GND}(f) + Z_{PN\ GND}(f)} + \frac{Z_{Ant}(f)}{Z_C(f)} \cdot \frac{U_0(f) \cdot Z_{PN\ GND}(f)}{Z_{TN\ GND}(f) + Z_{PN\ GND}(f)}. \quad (15)$$

By substitution of $U_0(f)$ in (15) with $I_{TN\ GND\ V}(f) \cdot Z_{TN\ GND}(f)$ for the first part of the right side, and with $I_{PN\ GND\ V}(f) \cdot Z_{PN\ GND}(f)$ for the second part, respectively, follows:

$$U_{Ant\ calc}(f) = \frac{Z_{Ant}(f)}{Z_C(f)} \cdot \frac{Z_{TN\ GND}(f) \cdot Z_{PN\ GND}(f)}{Z_{TN\ GND}(f) + Z_{PN\ GND}(f)} \cdot [I_{TN\ GND\ V}(f) + I_{PN\ GND\ V}(f)]. \quad (16)$$

TABLE I
COMPONENT VALUES FOR APPLIED SPICE SIMULATION

Component	Value	Description
C_{Ant}	10 pF	Monopole input capacitance
R_{Ant}	10 Meg Ω	Monopole input resistance
$Z_{TN\ GND}$	LISN LISN	HV LISN representation
$Z_{PN\ GND}$	30 nF	Common-mode parasitics of the three phases of the EME
C_{TN}	0.05–5 pF	Coupling capacitance of the TN
C_{PN}	0.05–5 pF	Coupling capacitance of the PN
C_C	0.1–10 pF	$C_{TN} + C_{PN}$, overall coupling capacitance

Equation (16) equals (12) with neglected $Z_{Ant}(f)$ in the denominator as all other parameters are unchanged and consistent. The combined TFs principle is not dependent on the impedance values $Z_{TN\ GND}(f)$ and $Z_{PN\ GND}(f)$. They do not influence its performance, no matter what values they have as long as they match between (12) and (16). The use of the superposition during the verification of the TFs presented is suitable, while $Z_C(f)$ is large compared to $Z_{Ant}(f)$. This is the case in real verification measurements. Otherwise, deviations between reference and calculation will occur. This constraint does not exist in a real active inverter setup because of the transient disturbance currents and the lack of a permanent short circuit between the TN and the PN as in the model of Fig. 10(c). Therefore, each network can be regarded as an independent radiator and the entire electric field strength can be calculated by the superposition of the two field parts. This leads to the theoretical correctness of the method for an active inverter. Hence, the implemented coupling capacitances in the TFs measured in (6) and (7) are the operative ones.

The verification of the model presented is performed using a SPICE simulation with schematics according to Fig. 10. Necessary impedances are chosen as shown in Table I. The coupling capacitors C_{TN} and C_{PN} are equal in a range of 0.05–5 pF. This allows to show the dependency of the calculated antenna voltages $U_{Ant\ calc}(f)$, according to (11), on the ratio between C_{Ant} and C_C influencing the assumption that $Z_C(f)$ is large compared to $Z_{Ant}(f)$. The TFs for the range of the coupling capacitors are calculated according to (9) and (10). As a reference, the antenna voltages are simulated as well as the currents $I_{TN\ GND\ V}(f)$ and $I_{PN\ GND\ V}(f)$ for the calculation of $U_{Ant\ calc}(f)$. Fig. 11 shows the maximum error between the antenna voltages $U_{Ant\ calc}(f)$ calculated and the simulated reference antenna voltages $U_{Ant\ V}(f)$ as a function of the ratio between C_{Ant} and C_C . With an increasing ratio, C_C becomes equal to C_{Ant} , meaning that $Z_{Ant}(f)$ is no longer small compared to $Z_C(f)$. This increases the maximum error from almost zero to 2.5 dB. Regarding realistic values for the capacitances mentioned, the ratio will be below 0.3 providing an error of a maximum of 1 dB. As a result, the calculation will reproduce the reference curve in shape with a tolerable amplitude error. This demonstrates the correctness of the model in combination with the TF method presented.

V. RUDIMENTARY EXPERIMENTAL TEST SETUP

A rudimentary nonshielded test setup is chosen for a first test of the combined TFs method on a real setup. A simple

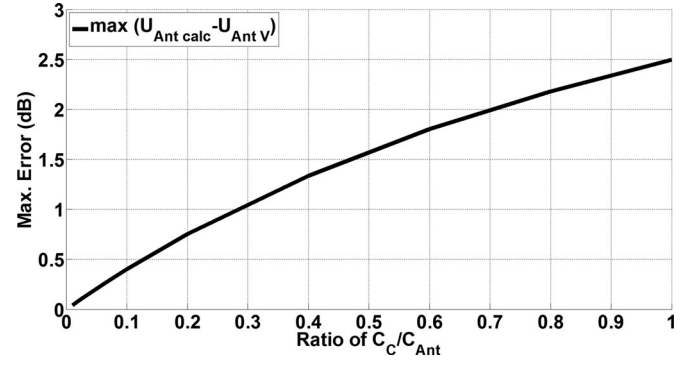


Fig. 11. Maximum error between the antenna voltage $U_{Ant\ calc}(f)$ calculated and the simulated antenna voltage $U_{Ant\ V}(f)$ of the electric model depending on the ratio of antenna capacitance C_{Ant} and coupling capacitance C_C .

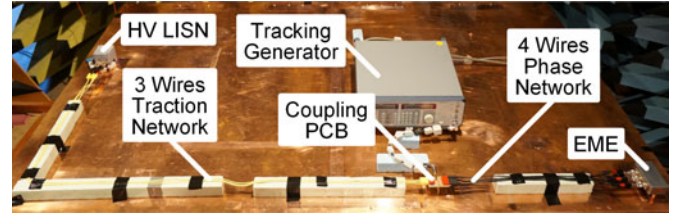


Fig. 12. Top view of the rudimentary setup.

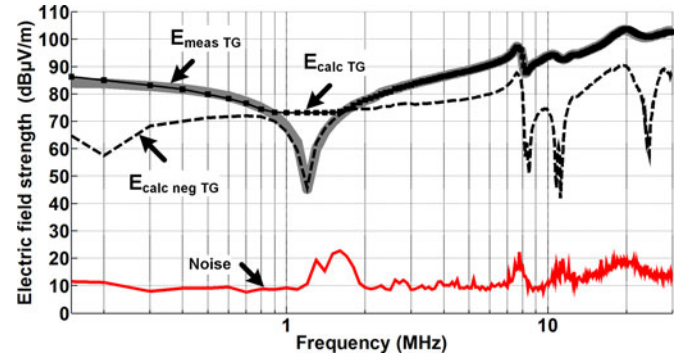


Fig. 13. Comparison of reference measurement $E_{meas\ TG}(f)$ to $E_{calc\ TG}(f)$ and $E_{calc\ neg\ TG}(f)$ for the verification purpose of the rudimentary setup excited by a tracking generator (TG).

coupling PCB representing an inverter with jacks for the TN and the PN is used. A signal generator can be coupled to the PCB via an SMA connector. Jumpers allow coupling of the inner conductor of the signal generator either with the TN, the PN, or both. The PCB can be considered either as an L piece or a T piece, depending on the jumper setting. An HV LISN replication and the EME presented are applied as loads for the networks. Laboratory single wires are used for the replication of unshielded interconnections. Three wires each 2 m long for the TN (T+, T-, and ground) and four wires each 1 m long for the PN (U, V, W, and ground) are used. Fig. 12 shows the setup.

TFs are generated and verification measurements are made according to Section IV. The comparison of the reference measurement and the result calculated is shown in Fig. 13. The agreement between the reference $E_{meas\ TG}(f)$ and the field

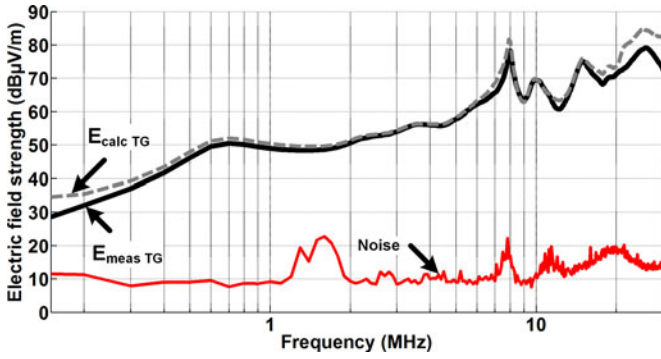


Fig. 14. Comparison of reference measurement $E_{\text{meas TG}}(f)$ to $E_{\text{calc TG}}(f)$ for the verification purpose of the electric drive system setup excited by a tracking generator (TG).

strength $E_{\text{calc TG}}(f)$ calculated is significant. A resonance is not replicated properly between 0.8 and 1.7 MHz. This resonance is caused by the EME. Because of the direct connection of the TN and PN during the verification in combination with a TG, which has no impressed voltage as for the SPICE simulation, the current on the TN is affected, leading to a 180° phase shift. This does not apply to a real inverter setup with transient signals. This imperfection can be solved for the verification measurement by a negative superposition of the two electric field components in the range of 0.8–1.7 MHz by (17) (see $E_{\text{calc neg TG}}(f)$ in Fig. 13). $E_{\text{calc neg TG}}(f)$ delivers the exact curve shape needed in between 0.8 and 1.7 MHz. This negative superposition represents a 180° phase shift occurring at the resonance frequency. The uneven noise floor is caused by the GPIB line communication into the shielded enclosure for the TG applied.

$$\begin{aligned} E_{\text{calc neg TG}}(f) &= E_{\text{calc TN}}(f) - E_{\text{calc PN}}(f) \\ &= TF_{\text{TN}}(f) \cdot I_{\text{TN GND TG}}(f) \\ &\quad - TF_{\text{PN}}(f) \cdot I_{\text{PN GND TG}}(f) \quad (17) \end{aligned}$$

VI. APPLICATION OF THE COMBINED TRANSFER FUNCTION TO AN ELECTRIC DRIVE SYSTEM SETUP

After the evaluation of the combined TF on the basis of a simplified, unshielded setup, the electric drive system setup presented previously is examined. The disturbance amplitudes expected are considerably smaller as a result of the entirely shielded HV system. For this system, a set of TFs is obtained, as described in Section IV. Verification measurements are performed and the result is presented in Fig. 14. The comparison between measurement $E_{\text{meas TG}}(f)$ and calculation $E_{\text{calc TG}}(f)$ shows a very good similarity. There are no major deviations besides 5 dB at the lower end and 10 dB at the upper end of the frequency range. The calculation without phase information and considering the setup as electrically small is a good approximation in the frequency range regarded. This result shows the applicability of the TF set generated for this kind of distributed system up to 30 MHz. With increasing frequency, the error will rise, due to neglected phase information for the TFs and

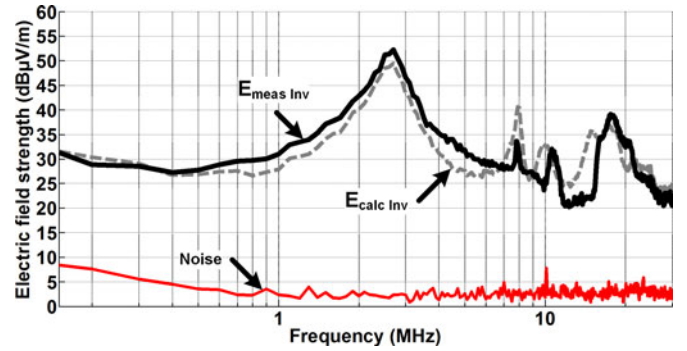


Fig. 15. Comparison of reference measurement $E_{\text{meas Inv}}(f)$ of the active inverter (Inv) in the electric drive system setup to the calculation $E_{\text{calc Inv}}(f)$.

the currents. Further, the setup will become electrically large, which leads to an inconstant current distribution along the harness. This current distribution cannot be represented by a single current probe measurement on each network.

After verification of the TFs, the method is applied to the setup with an active inverter (Inv). The internal power electronic of the inverter is connected with the terminals T+ and T- and the terminals U, V, and W. The LV harness is supplied with 12 V over the LISNs, and the TN with 24 V over the HV LISNs. The resulting ground disturbance currents are measured on the TN 0.5 m from the terminals T+ and T- and on the PN 0.25 m from the terminals U, V, and W as during the TFs generation. The electric field strength $E_{\text{meas Inv}}(f)$ is measured as the reference. With the verified TFs, the disturbance currents, and (8), the electric field $E_{\text{calc Inv}}(f)$ is calculated. The comparison between calculation and reference measurement is shown in Fig. 15. The calculation reproduces the shape and the tendency of the reference measurement very well. Minor deviations of a maximum of 7 dB can be observed up to 14 MHz. At 15 MHz, the maximum deviation is 13 dB. This result is satisfactory as a precompliance result. The prediction provides an overall impression of the disturbances expected and can indicate critical frequencies. Some deviations arise because of the inverter-driven transient and time-variant excitation of the networks in contrast to the sinusoidal signal during the verification procedure. This is because of the controlled mode in which the inverter is operated. Thus, peak currents and peak field strength measured must not necessarily correlate by using the TFs. This problem can be addressed by a time domain approach in the future. Here, simultaneous measurements of the ground currents on both networks and as reference of the electric field have to be performed. Time snapshots can then be transformed into the frequency domain. The calculation of the field can still be performed with (8). Additionally, the feedback of the current probe on the system has to be considered [21]. The influence on the electric field strength observed with and without current probe around the harness is at single frequency points at most 2 dB, for instance. Furthermore, the TF approach reduces the HV harnesses to a single conductor carrying the disturbance currents. In reality, currents are not equally distributed over the two or three coaxial cables, respectively. This is caused by the switching characteristic of the inverter's IGBTs.

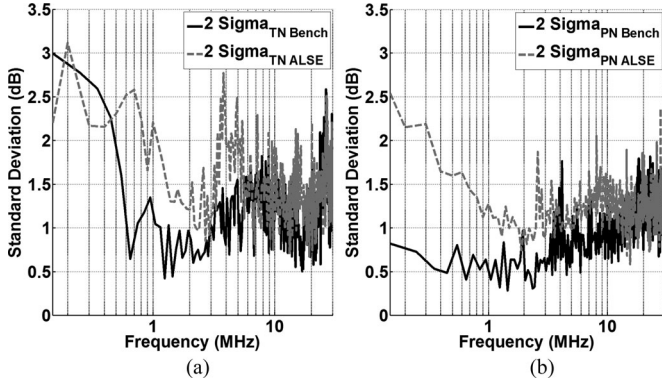


Fig. 16. Comparison of the standard deviation of ground currents of (a) the traction network and (b) the phase network in an ALSE setup and a bench setup.

VII. REPEATABILITY AND REPRODUCIBILITY OF CURRENT PROBE MEASUREMENTS

The precompliance method presented is based on current probe measurements. To ensure reliability of the method, it is important to know the deviations between the currents occurring in an ALSE setup and the currents occurring in a bench setup. In contrast to the ALSE setup, the laboratory setup available has a zinc-plated steel sheet as a table top instead of copper. There is no external irradiation on the laboratory setup influencing the current measurements. The setup is built up ten times in both environments. This time, the HV LISN is set up directly on the table tops without the copper bolt mentioned in Section II. The ground currents on the TN and on the PN are measured for each iteration. The operation mode of the inverter is a zero-ampere mode, as above in Section II. At first, the repeatability of the ground currents in an ALSE and on a bench is investigated. The plots in Fig. 16(a) and (b) show the two sigma standard deviations leading to a 95% confidence level for each of the ten current measurement sets on the TN and the PN. The maximum standard deviation is around 3 dB for the TN and 2.5 dB for the PN, which is low regarding the possible influences, such as the state of charge of the battery, changing contact resistances between the components, positioning of the whole setup on the tables, and positioning of the current probes. Therefore, measurement repeatability of this setup is granted in both environments.

Fig. 17 shows the mean values from the ten measurements of $I_{TN \text{ Mean Bench}}(f)$ and $I_{TN \text{ Mean ALSE}}(f)$ of the TN in (a) and $I_{PN \text{ Mean Bench}}(f)$ and $I_{PN \text{ Mean ALSE}}(f)$ of the PN in (b) for both setup environments. Both diagrams show a good agreement between the curves with maximum deviation of less than 2 dB. The reproducibility for ground currents in such a system in two different measurement environments is given. Hence, ground currents are a good basis for the precompliance method presented. This allows the application of the TF method in means of uncertainty as long as the TFs applied are correct.

VIII. EMC COUNTERMEASURES

To show the benefit of the method, EMC countermeasures are applied to a DUT and the combined TF method is applied. An inverter with the possibility to apply and remove the internal

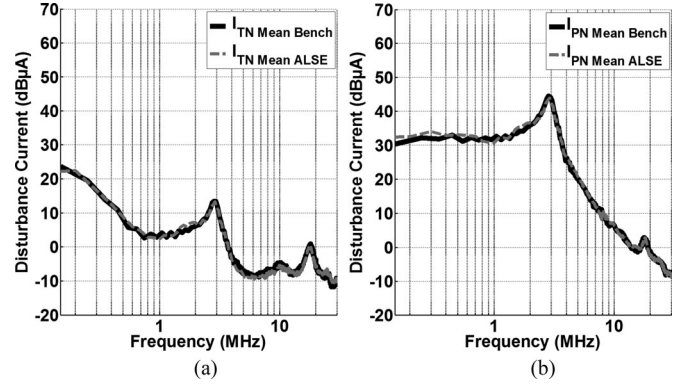


Fig. 17. Comparison of the mean values of ground currents of (a) the traction network and (b) the phase network in an ALSE setup and a bench setup.

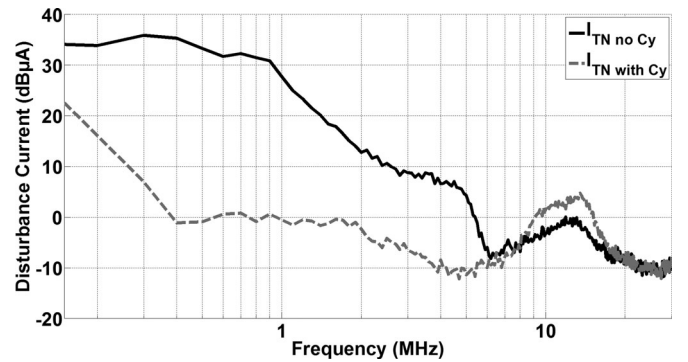


Fig. 18. Comparison of the disturbance currents on the traction harness with and without C_y capacitors.

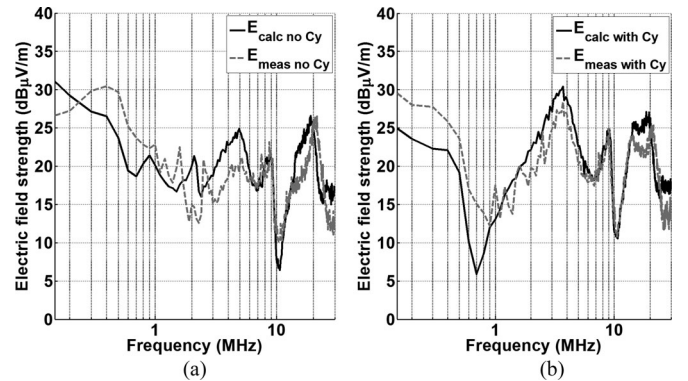


Fig. 19. Comparison of reference field measurements of the active inverter to the calculations (a) without C_y capacitors and (b) with C_y capacitors.

C_y capacitors acting as common-mode filters at the terminals of T+ and T- to ground (compare Fig. 3) is used. The setup is the same as described in Section II. TFs are generated and verified according to Section IV. Reference field and current measurements on the harness are performed with and without the C_y capacitors. The common-mode current on the TN can be decreased up to 30 dB using the mentioned filters as can be seen by comparison of $I_{TN \text{ no } C_y}(f)$ and $I_{TN \text{ with } C_y}(f)$ in Fig. 18. The comparison between measured and calculated electric field strength with and without applied C_y capacitors is shown in Fig. 19. Both calculations $E_{\text{calc no } C_y}(f)$ and $E_{\text{calc with } C_y}(f)$

have a good agreement compared with their reference measurements $E_{\text{meas no } C_y}(f)$ and $E_{\text{meas with } C_y}(f)$. The deviations are mainly lower than 5 dB. Positive and negative effects of the common-mode filtering can be calculated. Around 0.7 MHz the field strength is decreased by 15 dB through the application of the filter, the effect which was intended. Around 4 MHz an unintentional increase of 7.5 dB can be observed. This example shows the applicability of the method for common-mode interference countermeasures.

IX. CONCLUSION

A combined TF method is introduced and explained for distributed systems. It allows the estimation of radiated emissions during a component test according to CISPR 25 without the need for an ALSE. It is applied to an automotive electric drive system with dominating common-mode emissions. A test setup for characterizing an HV inverter's EMC performance is presented. The relevant disturbance currents and paths in such a system are explained in detail and the coupling mechanism to an antenna is modeled. The results for verification and validation of the combined TF method show a good agreement to measurements throughout the frequency range investigated. The tendency and shape of reference measurements compared to the calculation differ with a maximum of 13 dB in the electric field strength. The precompliance results obtained give a very good and reproducible estimation of the expectable radiated emissions. It can indicate upcoming issues and show the impact of applied common-mode filtering to the DUT. Hence, it fulfills its designation as a tool supporting the EMC engineer's work, with the advantage of saving time and money. In the future, the combined TF method has to be applied to different operation modes of the inverter and to different EMC solutions within the drive system showing its limits. A time-domain approach will improve the accuracy as well as the consideration of differential-mode interferences.

ACKNOWLEDGMENT

The authors would like to thank Robert Bosch GmbH for the supply of measurement equipment and components. They would also like to thank R. Eidher and S. Nishizawa from the Robert Bosch GmbH for their support.

REFERENCES

- [1] I. E. Commission, "CISPR 25 Ed.3: Vehicles, boats and internal combustion engines—Radio disturbance characteristics—Limits and methods of measurement for the protection of on-board receivers," 2008.
- [2] R. Videnka and J. Svacina, "Introduction to EMC pre-compliance testing," in *Proc. 17th Int. Conf. Microw., Radar Wireless Commun.*, May 19–21, 2008, pp. 1–4.
- [3] C. Paul, *Introduction to Electromagnetic Compatibility*. New York, NY, USA: Wiley, 1992.
- [4] F. Costa, C. Gautier, B. Revol, J. Genoulaz, and B. Demoulin, "Modeling of the near-field electromagnetic radiation of power cables in automobiles or aeronautics," *IEEE Trans. Power Electron.*, vol. 28, no. 10, pp. 4580–4593, Oct. 2013.
- [5] U. Reggiani, A. Massarini, L. Sandrolini, M. Ciccotti, X. Liu, D. Thomas, and C. Christopoulos, "Experimental verification of predicted electromagnetic fields radiated by straight interconnect cables carrying high-

frequency currents," presented at the 2003 IEEE Bologna Power Tech. Conf., Bologna, Italy, Jun. 23–26, 2003.

- [6] M. Di Piazza, A. Ragusa, G. Tine, and G. Vitale, "A model of electromagnetic radiated emissions for dual voltage automotive electrical systems," in *Proc. IEEE Int. Symp. Ind. Electron.*, 2004, vol. 1, pp. 317–322.
- [7] J. Wang, O. Fujiwara, and K. Sasabe, "A simple method for predicting common-mode radiation from a cable attached to a conducting enclosure," in *Proc. Asia-Pacific Microw. Conf.*, 2001, vol. 3, pp. 1119–1122.
- [8] D. Schneider, S. Tenbohlen, and W. Köhler, "Untersuchung von vorhergesagtem abstrahlung bei komponententests nach CISPR 25," in *Proc. EMV, Düsseldorf, Germany*, 2012, pp. 263–271.
- [9] F. Tesche, M. Ianoz, and T. Karlsson, *EMC Analysis Methods and Computational Models*. New York, NY, USA: Wiley, 1997.
- [10] A. Radchenko, V. Khilkevich, N. Bondarenko, D. Pommerenke, M. Gonsler, J. Hansen, and C. Keller, "Transfer function method for predicting the emissions in a CISPR-25 test-setup," *IEEE Trans. Electromagn. Compat.*, vol. PP, no. 99, pp. 1–9, Jan. 2014.
- [11] W. Smith and R. Frazier, "Prediction of anechoic chamber radiated emissions measurements through use of empirically-derived transfer functions and laboratory common-mode current measurements," in *Proc. IEEE Int. Symp. Electromagn. Compat.*, 1998, vol. 1, pp. 387–392.
- [12] D. Schneider, M. Böttcher, S. Tenbohlen, and W. Köhler, "Pre-compliance test method for radiated emissions with multiple segment transfer functions," in *Proc. IEEE Int. Symp. Electromagn. Compat.*, Aug. 2013, pp. 605–610.
- [13] D. Schneider, M. Böttcher, B. Schoch, S. Hurst, S. Tenbohlen, and W. Köhler, "Transfer functions and current distribution algorithm for the calculation of radiated emissions of automotive components," in *Proc. Int. Symp. Electromagn. Compat.*, Sep. 2013, pp. 443–448.
- [14] S. Guttowski, S. Weber, E. Hoene, W. John, and H. Reichl, "EMC issues in cars with electric drives," in *Proc. IEEE Int. Symp. Electromagn. Compat.*, Aug. 18–22, 2003, pp. 777–782.
- [15] D. Schneider, M. Böttcher, S. Tenbohlen, and W. Köhler, "Estimation of radiated emissions of an automotive HV-inverter in a distributed system," presented at the Int. Symp. Electromagn. Compat., Tokyo, Japan, May 2014.
- [16] M. Reuter, T. Friedl, S. Tenbohlen, and W. Köhler, "Emulation of conducted emissions of an automotive inverter for filter development in HV networks," in *Proc. IEEE Int. Symp. Electromagn. Compat.*, Aug. 2013, pp. 236–241.
- [17] C. Holloway, E. Kuester, A. Ruehli, and G. Antonini, "Partial and internal inductance: Two of Clayton R. Paul's many passions," *IEEE Trans. Electromagn. Compat.*, vol. 55, no. 4, pp. 600–613, Aug. 2013.
- [18] C. Jettanasen, "Influence of power shielded cable and ground on distribution of common mode currents flowing in variable-speed AC motor drive system," in *Proc. Asia-Pacific Symp. Electromagn. Compat.*, Apr. 12–16, 2010, pp. 953–956.
- [19] C. Paul, "A comparison of the contributions of common-mode and differential-mode currents in radiated emissions," *IEEE Trans. Electromagn. Compat.*, vol. 31, no. 2, pp. 189–193, May 1989.
- [20] K. L. Kaiser, *Electromagnetic Shielding*. Boca Raton, FL, USA: CRC Press, 2005.
- [21] R. Chundru, D. Pommerenke, and S. Chandra, "A new calibration method for current probes," in *Proc. Int. Symp. Electromagn. Compat.*, Aug. 2004, vol. 1, pp. 163–168.



Daniel Schneider received the Diploma in electrical engineering from the University of Stuttgart, Stuttgart, Germany, in 2009.

He is currently a Research Assistant at the Institute of Power Transmission and High Voltage Technology, University of Stuttgart. His current research interests include the measurement technique of electromagnetic compatibility, especially in the area of the automotive component test.



Michael Beltle received the Dipl.-Ing. degree in electrical engineering from the University of Stuttgart, Stuttgart, Germany, in 2009.

In his diploma thesis, he was involved in determining degrading effects of electrostatic discharges on microcontrollers in automotive applications. He has been an Academic Researcher with the Institute of Power Transmission and High Voltage Technology, University of Stuttgart, where he is involved in the field of power transformer diagnostics and determines the long-term development of partial discharges and investigates the mechanical vibrations of active parts of transformers.

Mr. Beltle is a Member of CIGRE and the German Power Engineering Society VDE-ETG.



Martin Siegel received the Dipl.-Ing. degree in electrical engineering from the University of Stuttgart, Stuttgart, Germany, in 2010.

In his diploma thesis, he was involved in the integration of electric vehicles in a grid with a high proportion of renewable energies. Since 2011, he has been an Academic Researcher at the Institute of Power Transmission and High Voltage Technology, University of Stuttgart, where he operates in the field of power transformer diagnostics and monitoring. His current research interests include applicability of un-

conventional partial discharge measurement methods for online monitoring and localization at power transformers.

Mr. Siegel is a Member of the German Power Engineering Society VDE-ETG.



Stefan Tenbohlen (M'07) received the Diploma and Dr.-Ing. degree from the Technical University of Aachen, Germany, in 1992 and 1997, respectively.

In 1997, he joined AREVA Schorch Transformatoren GmbH, Mönchengladbach, Germany, where he was responsible for basic research and product development, and with this function, he was involved in the field of online monitoring of power transformers. From 2002 to 2004, he was the Head of the Electrical and Mechanical Design Department. In 2004, he was the Professor and Head of the Institute of Power

Transmission and High Voltage Technology, University of Stuttgart, Stuttgart, Germany. His current research interests include diagnostic of equipment of electrical networks, development of high-voltage measurement technique, behavior of gas-insulated insulation systems, and different aspects of automotive electromagnetic compatibility. He holds several patents and published more than 130 papers.

Prof. Tenbohlen is a Member of the German committees of CIGRE A2 (Power Transformers), D1 (Emerging Technologies), C4 (System Technical Performance), and several international working groups. Since 2008, he has been a Member of the Board of the German Power Engineering Society VDE-ETG.



Wolfgang Köhler received the Dipl. and the Dr.-Ing. degree in electronic engineering from the University of Stuttgart, Stuttgart, Germany, in 1981 and 1988, respectively.

Since 1981, he has been with the Institute of Power Transmission and High Voltage Technology, University of Stuttgart, where he is currently the Head of the High-Voltage Laboratory. His current research interests include automotive EMC and high-voltage testing and measurement. He also gives lectures on EMC and in high-voltage testing and measurements.